

## Structure-oriented bilateral filtering of seismic images

Dave Hale, Center for Wave Phenomena, Colorado School of Mines

### SUMMARY

Bilateral filtering is widely used to enhance photographic images, but in most implementations is poorly suited to seismic images. A bilateral filter consists of two (domain and range) filter kernels. By replacing the domain kernel with a smoothing filter that conforms to image structures, we obtain a bilateral filter suitable for seismic image processing. Examples and comparison with conventional edge-preserving smoothing illustrate advantages of structure-oriented bilateral filtering. The only significant disadvantage is a relatively high (roughly 10 to 40 times higher) computational cost.

### INTRODUCTION

Bilateral filters (Tomasi and Manduchi, 1998) are today widely used to smooth photographic images while preserving significant edges. Paris et al. (2008) provide a thorough review of bilateral filters and their applications, which include denoising, image abstraction, and texture and tone adjustment. Despite such widespread application to photographic images (and to medical CT and MRI scans), bilateral filters are seldom used to enhance seismic images. Why not?

One reason is that edges in seismic images differ significantly from those in photographic images (and in medical CT or MRI scans). Consider for example the seismic image displayed in Figure 1a. The most obvious edges in this image are the familiar alternating black and white features that correspond to seismic horizons. However, these sinusoidal features are unlike the edges apparent in most photographs. Rather, features in Figure 1a correspond to reflections of seismic waves caused by changes in seismic impedance. Edges in images of seismic impedance, when such images are available, more closely resemble edges in photographs.

Also important are edges corresponding to lateral discontinuities in seismic reflections, the chaotic structures at about 1.2 s and the geologic faults below 1.5 s in the image of Figure 2a. (Figure 1a is a zoomed subset of Figure 2a). In processing seismic images, we seek to denoise (enhance the continuity of) coherent reflections, while preserving these lateral discontinuities.

The anisotropic diffusion filter (Weickert, 1999; Fehmers and Höcker, 2003) is one example of a filter that does this for seismic images, as well as for photographic images. Indeed, others have compared the anisotropic diffusion filter with the bilateral filter in processing to enhance photographs (e.g., Barash, 2002). In this paper I compare the implementation and performance of these two types of filters in denoising seismic images, using a new structure-oriented bilateral filter that accounts for the different types of edges apparent in such images.

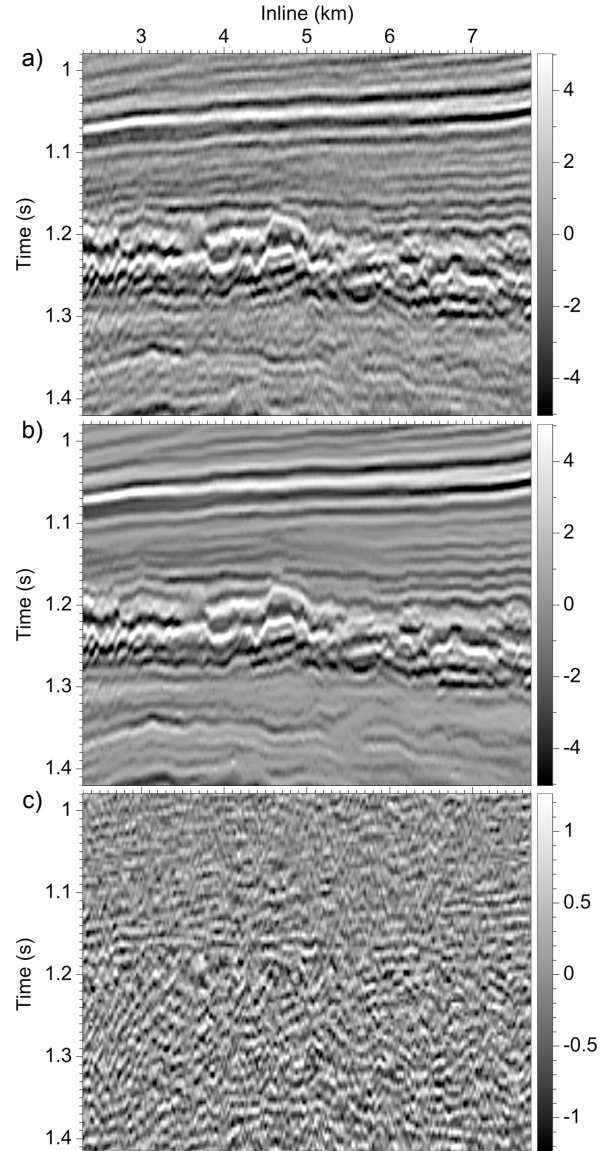


Figure 1: An input seismic image (a), the output of structure-oriented bilateral filtering (b), and the difference (c) between input and output images. For clarity, the input-output difference is displayed for a smaller gray-scale range of amplitudes.

### STRUCTURE-ORIENTED SMOOTHING

Let  $p[\mathbf{i}]$  and  $q[\mathbf{i}]$  denote input and output images, respectively, where  $\mathbf{i} = (i_1, i_2, \dots, i_n)$  is an  $n$ -dimensional sample index with  $n$  integer components. A general smoothing filter can then be

## Structure-oriented bilateral filtering

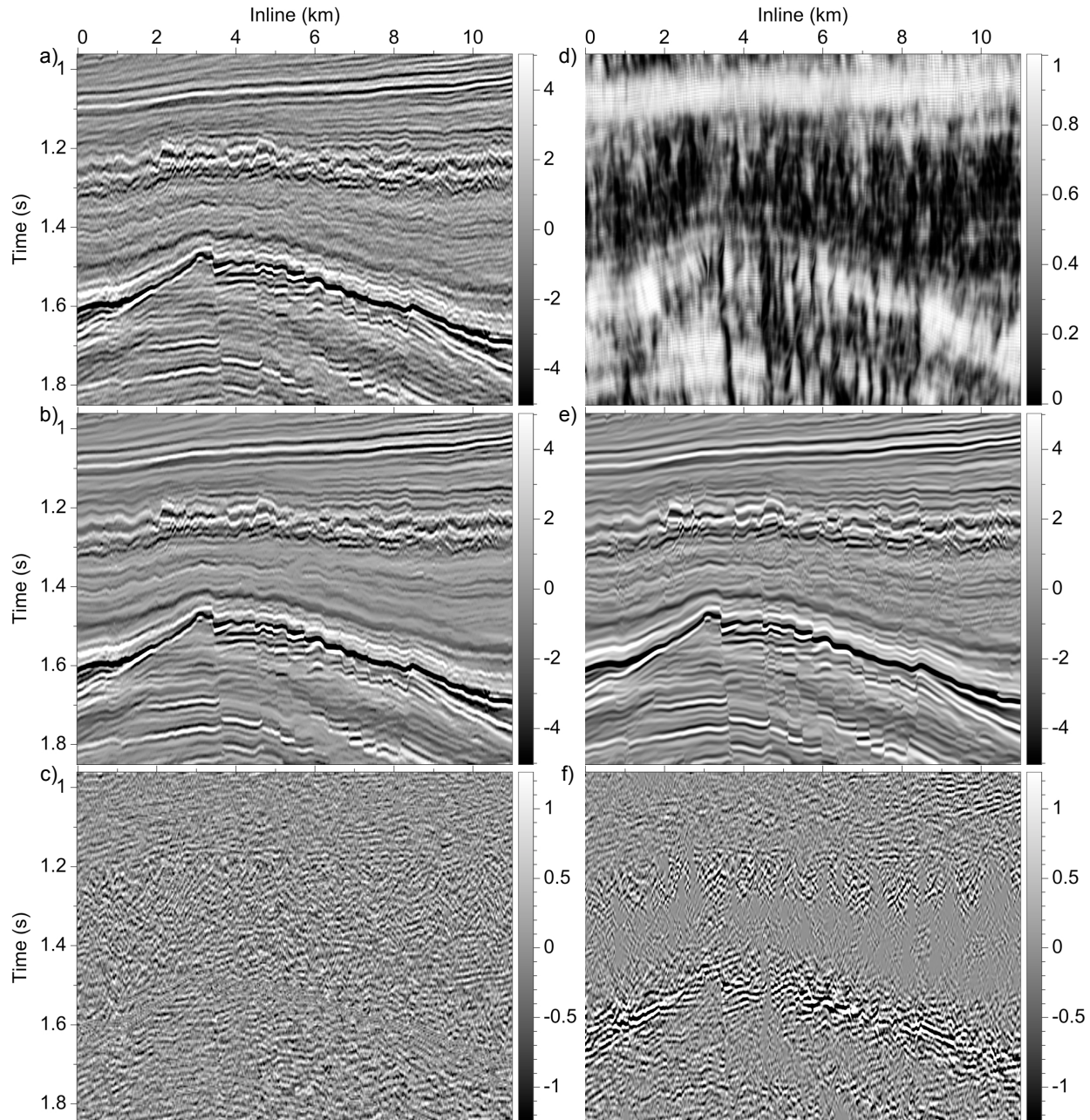


Figure 2: An input image (a), with output (b) and input-output difference (c) for the structure-oriented bilateral filter. For comparison, coherence (d) is computed to implement a more conventional edge-preserving smoothing filter, with output (e) and input-output difference (f).

## Structure-oriented bilateral filtering

expressed as follows:

$$q[\mathbf{i}] = \frac{\sum_j p[\mathbf{j}] s(\mathbf{i}, \mathbf{j})}{\sum_j s(\mathbf{i}, \mathbf{j})}. \quad (1)$$

This smoothing filter is not shift-invariant (not convolutional) because the coefficients  $s(\mathbf{i}, \mathbf{j})$  vary spatially with both output and input sample indices  $\mathbf{i}$  and  $\mathbf{j}$ , as necessary to conform to structures apparent in seismic images. Division by the sum of these coefficients in equation 1 ensures that smoothing of an input image  $p[\mathbf{i}] = \text{constant}$  (already smooth as can be) yields an identical output image  $q[\mathbf{i}] = \text{constant}$ .

In practice we need not compute the coefficients  $s(\mathbf{i}, \mathbf{j})$  explicitly. Instead, to smooth *along* structures apparent in images, without smoothing *across* those structures, I solve a discrete approximation to the following partial differential equation:

$$q(\mathbf{x}) - \frac{\sigma^2}{2} \nabla \cdot \mathbf{D}(\mathbf{x}) \cdot \nabla q(\mathbf{x}) = p(\mathbf{x}), \quad (2)$$

for tensor-valued filter coefficients  $\mathbf{D}(\mathbf{x})$ . Here,  $\mathbf{x}$  represents coordinates in space or space-time that when sampled become indices  $\mathbf{i}$  and  $\mathbf{j}$  in equation 1.

Solution of this equation approximates Gaussian smoothing with half-width  $\sigma$  in the directions of eigenvectors of  $\mathbf{D}(\mathbf{x})$  for which corresponding eigenvalues equal one. By choosing those directions to be tangent to structures apparent in an input image  $p$ , and by choosing eigenvalues for orthogonal directions to be much less than one, smoothing is oriented along image structures. The filters used in the examples of Figures 1 and 2 have a maximum smoothing half-width of  $\sigma = 16$  samples (0.4 km or 0.064 s).

Solving equation 2 is similar to applying coherence-enhancing anisotropic diffusion (Weickert, 1999; Fehmers and Höcker, 2003). As for that process, I derive the tensor-valued coefficients  $\mathbf{D}(\mathbf{x})$  from structure tensors computed for the input image.

### Edge-preserving smoothing

To preserve edges while smoothing, we may scale the tensors  $\mathbf{D}(\mathbf{x})$  by any measure of coherence that is almost zero near discontinuities and almost one where features are most coherent. In effect, scaling by coherence reduces the maximum half-width  $\sigma$  of the smoothing filter by a factor that varies spatially; that is, it makes the smoothing filter edge-preserving.

Figure 2e shows the effect of edge-preserving structure-oriented smoothing with equation 2, using tensors  $\mathbf{D}(\mathbf{x})$  scaled by coherence displayed in Figure 2d. Near discontinuities, such as faults, coherence is low and little smoothing is performed. Smoothing near but not across discontinuities appears to enhance the definition of faults in the output image  $q$  of Figure 2e.

The input-output difference in Figure 2f indicates that little smoothing is performed near the middle of the image, at times near 1.4 s, where features in the input image  $p$  are least coherent. Note, however, that the largest differences in Figure 2f exhibit significant spatial correlation, and that these differences coincide with high amplitudes.

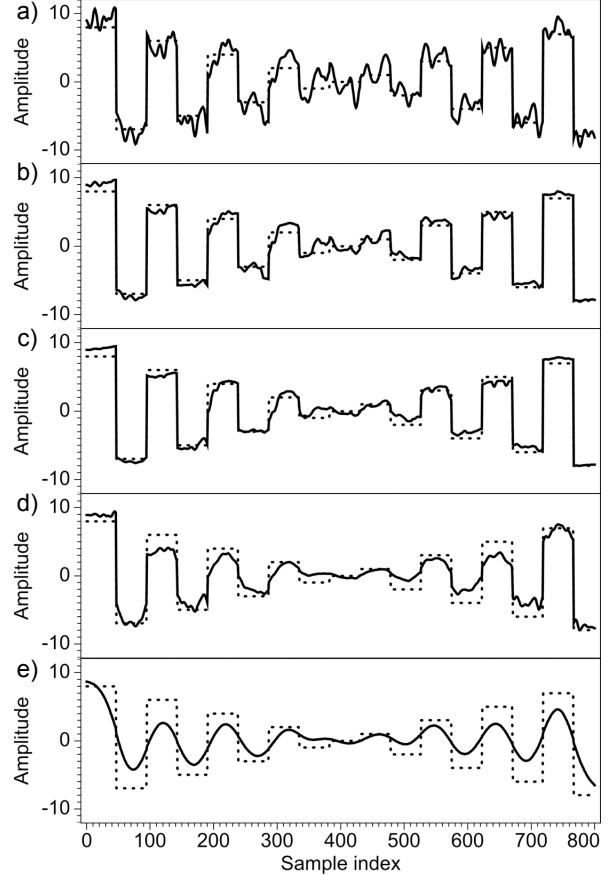


Figure 3: Bilateral filtering of a blocky signal (dashed lines) contaminated with additive random noise. The smoothing filter kernel is Gaussian with half-width  $\sigma = 20$  samples. Half-widths  $\sigma_p$  of the Tukey range filter kernel are (a) 1/100, (b) 1/2, (c) 1, (d) 3/2, and (e) 10 times the value  $\sigma_p \approx 4$  given by equation 5.

## BILATERAL FILTERING

The name *bilateral filter* (Tomasi and Manduchi, 1998) was chosen to imply that the kernel of this filter is a combination of two filter kernels, one a function of the input image's spatial *domain* and the other a function of its *range*. The basic idea is simple. We modify the general smoothing filter equation 1 to scale the coefficients  $s(\mathbf{i}, \mathbf{j})$  by a range function  $r(p[\mathbf{i}] - p[\mathbf{j}])$  of the difference between two input sample values:

$$q[\mathbf{i}] = \frac{\sum_j p[\mathbf{j}] r(p[\mathbf{i}] - p[\mathbf{j}]) s(\mathbf{i}, \mathbf{j})}{\sum_j r(p[\mathbf{i}] - p[\mathbf{j}]) s(\mathbf{i}, \mathbf{j})}. \quad (3)$$

The range function  $r(p)$  should be chosen to decrease monotonically with increasing  $|p|$ . In practice (Durand and Dorsey, 2002), a simple and effective choice is Tukey's biweight function, defined by

$$r(p) \equiv \begin{cases} [1 - (p/\sigma_p)^2]^2 & \text{if } |p| < \sigma_p, \\ 0 & \text{otherwise.} \end{cases} \quad (4)$$

## Structure-oriented bilateral filtering

The half-width  $\sigma_p$  of the range function  $r$  controls the scaling of the spatial filter coefficients  $s$  in equation 3. In practice, I find that a good choice is

$$\sigma_p \approx p_{75} - p_{25} \quad (5)$$

where  $p_{25}$  and  $p_{75}$  denote the 25'th and 75'th percentiles (1st and 3rd quartiles) of the sample values in the input image  $p$ .

Figure 3 illustrates for a synthetic example the effect that the half-width  $\sigma_p$  has on bilateral smoothing. For small values of  $\sigma_p$ , little smoothing is performed, because then only values  $p[j] \approx p[i]$  are averaged by equation 3 when computing the output value  $q[i]$ . For large values of  $\sigma_p$ , scaling by the range function has little effect, and the bilateral filter is merely a spatial smoothing filter, one that does not preserve edges. For a range of intermediate values  $2 < \sigma_p < 6$ , the bilateral filter attenuates noise while more or less preserving edges in the signal. This synthetic example explains the effectiveness of the bilateral filter when applied to photographs or medical images with similar step edges.

Recall, however, that edges most apparent in seismic images are reflections with sinusoidal waveforms, which are not step functions. When applied to seismic images, simple implementations of the bilateral filter preserve faults and other discontinuities, but attenuate both coherent signal and incoherent noise. This fact alone may explain why the bilateral filter is rarely used in seismic image processing.

### Structure-oriented bilateral filtering

Typical implementations of the bilateral filter fail when applied to seismic images, because, unlike structure-oriented smoothing, they smooth too much across seismic reflections. Therefore, *for structure-oriented bilateral filtering, we may simply replace the smoothing filter kernel  $s(i,j)$  with structure-oriented smoothing*.

Remember that the filter coefficients  $s(i,j)$  are not computed explicitly. Instead, we apply the spatial smoothing filter by solving the partial differential equation 2. Because the range filter kernel  $r$  is a function of both output and input indices  $i$  and  $j$ , an efficient implementation of equation 3 may not be obvious.

My implementation is similar to that of Durand and Dorsey (2002). Specifically, I use a piecewise linear approximation of the range function  $r(p)$ , for a finite number  $N_p$  of values  $p_k = p_{min} + k\Delta p$ , for  $k = 0, 1, \dots, N_p - 1$ , where

$$N_p = 2 + \left\lfloor \frac{p_{max} - p_{min}}{\sigma_p} \right\rfloor \quad (6)$$

and

$$\Delta p = \frac{p_{max} - p_{min}}{N_p - 1}. \quad (7)$$

For this piecewise-linear approximation of the range function  $r$ , equation 3 becomes

$$q[i] = \frac{\sum_k \Lambda(p[i] - p_k) \sum_j p[j] r(p[j] - p_k) s(i,j)}{\sum_k \Lambda(p[i] - p_k) \sum_j r(p[j] - p_k) s(i,j)}, \quad (8)$$

where  $\Lambda(p[i] - p_k)$  is a shifted version of the hat function defined by

$$\Lambda(p) \equiv \begin{cases} 1 - \frac{|p|}{\Delta p} & \text{if } |p| < \Delta p, \\ 0 & \text{otherwise.} \end{cases} \quad (9)$$

Note that the  $\sum_j$  terms in the numerator and denominator of equation 8 resemble those in equation 1. In equation 1 these terms represent structure-oriented smoothing of the images  $p[j]$  and 1 (a constant image). In equation 8 these terms imply exactly the same smoothing of images  $p[j]r(p[j] - p_k)$  and  $r(p[j] - p_k)$ . For all of these images, we perform spatial smoothing by solving the partial differential equation 2.

Figure 2b displays the result of structure-oriented bilateral filtering of the image in Figure 2a. Faults and other discontinuities are well-preserved in the output image; and the input-output difference shown in Figure 2c exhibits less spatial correlation than is observed for edge-preserving smoothing.

Structure-oriented bilateral filtering preserves faults and other sharp discontinuities in Figure 2a, *without using any prior estimate of coherence*. Instead, the range function of the bilateral filter inhibits smoothing across a fault where values on each side of the fault differ significantly. As others have noted (e.g., Paris et al., 2008), this simplicity of the bilateral filter is one of its advantages.

For this example, I used  $N_p = 19$ , which implies that a total of  $2N_p = 38$  structure-oriented smoothings were performed, 19 for the numerator and 19 for the denominator of equation 8. This rather large number  $N_p = 19$  is necessary for the image of Figure 2a because for this image  $p_{min} \ll p_{25}$  and  $p_{75} \ll p_{max}$ . For images with more balanced amplitudes, the number  $N_p$  is lower, typically less than 10.

## CONCLUSION

On the one hand, structure-oriented bilateral filtering requires many more solutions to equation 2 than the one solution required for edge-preserving structure-oriented smoothing. Relatively high computational cost is therefore a disadvantage of my implementation of structure-oriented bilateral smoothing.

On the other hand, edge-preserving smoothing requires an estimate of coherence to inhibit smoothing across faults and other geologically significant discontinuities. The effectiveness of edge-preserving smoothing depends on this prerequisite image of coherence.

Bilateral filtering requires only the input image, and the noise removed by the filter (the input-output difference), tends to be more uniformly distributed and to exhibit less spatial correlation than that removed by edge-preserving smoothing.

## ACKNOWLEDGMENT

Thanks to dGB Earth Sciences B.V., for providing (through OpendTect), the seismic image displayed in Figures 1a and 2a.

## Structure-oriented bilateral filtering

### REFERENCES

- Barash, D., 2002, A fundamental relationship between bilateral filtering, adaptive smoothing and the nonlinear diffusion equation: *IEEE Transactions on Pattern Analysis and Machine Intelligence*, **24**, 1–5.
- Durand, F., and J. Dorsey, 2002, Fast bilateral filtering for the display of high-dynamic-range images: *ACM Transactions on Graphics*, **21**, 257–266.
- Fehmers, G., and C. Höcker, 2003, Fast structural interpretation with structure-oriented filtering: *Geophysics*, **68**, 1286–1293.
- Paris, S., P. Kornprobst, J. Tumblin, and F. Durand, 2008, A gentle introduction to bilateral filtering and its applications: *ACM SIGGRAPH 2008 classes*, ACM, 1–50.
- Tomasi, C., and R. Manduchi, 1998, Bilateral filtering for gray and color images: *Proceedings of the Sixth International Conference on Computer Vision (ICCV 98)*, IEEE Computer Society, 839.
- Weickert, J., 1999, Coherence-enhancing diffusion filtering: *International Journal of Computer Vision*, **31**, 111–127.